Rare Metal Materials and Engineering
Volume 51, Issue 4, April 2022
Available online at www.rmme.ac.cn

Science Press

Cite this article as: Chen Li, Li Yuluo, Shen Ningning, et al. 3-D Steady Time-Independent Simulation on the Fluid Flow Field and Heat Transfer of Cooling Roller During Planar Flow Casting Process[J]. Rare Metal Materials and Engineering, 2022, 51(04): 1211-1217.

ARTICLE

3-D Steady Time-Independent Simulation on the Fluid Flow Field and Heat Transfer of Cooling Roller During Planar Flow Casting Process

Chen Li, Li Yuluo, Shen Ningning, Hui Xidong

State Key Laboratory for Advanced Metals and Materials, University of Science and Technology Beijing, Beijing 100083, China

Abstract: Planar flow casting (PFC) is an advanced technology to produce amorphous and nanocrystalline ribbons in electrical application. One of the major challenges of this technology is not only to have a rapid cooling rate to suppress the crystallization but also to achieve a high surface quality of ribbons. A new way to predict the fluid flow fields and heat transfer coefficient distribution of two types of single-roll cooling structures which are widely used in industrial production was proposed, i. e. 3-D time-independent steady simulation models. The flow velocity distribution of the two types of structures was calculated by software FLUENT, combined with energy and momentum equations. Additionally, the convective heat transfer coefficient distribution of the two structures was predicated. The results show that the velocity distribution of the roller with a water channel structure (WCS) is neither uniform nor periodic, and that of the roller with a water gap structure (WGS) is not uniform but periodic. The convective heat transfer coefficient distribution of the two kinds of rollers is not centrally symmetric, and the cooling feature of WGS roller is more regular. Three appropriate zones with symmetric distribution were predicated for a WGS roller, which was verified by the succeeding times of continuous production of ribbons. According to the thermal equilibrium principle, the heat transfer process of PFC technology was also described. These data suggest that uniform distribution of convective heat transfer coefficient can be one of the criterions to design the structure of cooling roller.

Key words: planar flow casting; numerical simulation; fluid flow field; heat transfer; amorphous and nanocrystalline alloys

Amorphous and nanocrystalline (AM/NC) alloys have attracted increasing attention as a new generation of soft magnetic materials due to their superior high saturation magnetization and low coercivity, as well as core loss at both high frequency and no-load state compared to classical silicon or ferrite steel. AM/NC alloys are used in a wide range of industry fields, such as in transformers, pulse power devices, sensors and telecommunication devices[1-3]. Superior torque motors with an amorphous core in new electric vehicles for large capacity applications have been thoroughly investigated in recent years[4]. NC ribbons have been considered the best materials in wireless power transfer field because of their high charging efficiency[5].

The planar flow casting (PFC) method invented by Narasimhan[6] is a breakthrough method for fabricating amorphous ribbons. Fig.1 illustrates the schematic of the PFC process. In the process, molten metal is ejected from a crucible through a rectangle nozzle slot onto a cooling roller. A puddle constrained by the surface tension is then formed between the nozzle and the cooling roller, which adheres to substrate wheel, and is rapidly solidified into ribbon. Then the ribbon is detached from the roller by air blower near 1/4 of a rotation circle[7].

Many studies have been conducted to analyze the PFC process since 1979. Until now, most of the studies use experimental or computational simulation methods to focus on the melt puddle or the interface between the cooling wheel and puddle[8-15]. Little work has been done on the effect of internal geometric structure of cooling roller on the fluid flow fields during PFC process. This is important, as the design of

Received date: April 22, 2021
Foundation item: National Key Research and Development Program of China (2016YFB0300502); National Natural Science Foundation of China (51801230); Key Project of the Equipment Pre-Research Field Fund of China (6140922010302)
Corresponding author: Hui Xidong, Ph. D., Professor, State Key Laboratory for Advanced Metals and Materials, University of Science and Technology Beijing, Beijing 100083, P. R. China, Tel: 0086-10-62333066, E-mail: xdhui@ustb.edu.cn

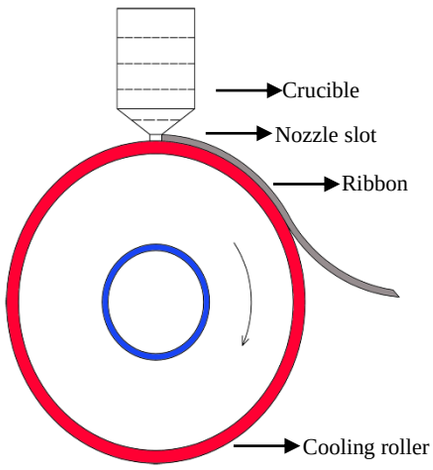

Fig.1 Schematic of the PFC process

the cooling system plays a critical role in the PFC process to achieve amorphous alloys and high quality of ribbon. The fluid flow field directly determines the temperature fields and the cooling rates at different positions, which then affects the formation of amorphous structure and internal stress.

Therefore, this work aims to formulate the distribution of the fluid flow field of two typical cooling structures using 3-D steady time-independent simulation models. Meanwhile, the convective heat transfer coefficient is also calculated as a variable quantity at the interface of the water and the cooling roller. The width of the ribbon and the proper position of producing ribbon upon the cooling roller were predicted, which was in agreement with the ribbon width in industrial production. Finally, the design criterion for cooling structure based on the thermal equilibrium principle was established.

1 Models and Calculation Methods

1.1 Calculation models

The models are formulated based on the following assumptions.

(1) The mathematic model of the cooling structure is three-dimensional and in a steady-state simulation.

(2) Since the heat expansion of the cooling roller is much smaller than the diameter, the dimensional change of the cooling roller is negligible. The cooling roller is assumed to be a round ring.

(3) When liquid flows in cooling structure, it comes into a no-penetration and no-slip boundary condition.

(4) Liquid inlet rate (Q) and temperature (T) are constant.

(5) The cooling water is incompressible and Newtonian liquid.

(6) The water flow is turbulent because the Reynolds number of cooling water in the cooling structure is much bigger than 2300.

(7) The viscosity of the cooling water is constant considering that the temperature difference is negligible from the inlet pipe to the outlet pipe.

(8) Radiative heat transfer is ignored in this simulation.

The above assumptions are applied for the construction of calculation models of two types of structures, which have a steady-state, incompressible, turbulence flow problem with the cooling wall. The velocity and pressure fields are coupled accurately by solving the Navier-Stokes momentum equation, and temperature field can be calculated with the energy equation. Finally, the results are checked by the continuity equation. The basic governing equations in the simulation are presented as follows:

(1) Continuity equation:

$$\frac{\partial \rho}{\partial t} + \frac{\partial (\rho u_i)}{\partial x_i} = 0 \tag{1}$$

where ρ is independent with time based assumption (5), and hence

$$\frac{\partial \rho}{\partial t} = 0 \tag{2}$$

Combining Eq.(1) with Eq.(2):

$$\frac{\partial u_i}{\partial x_i} = 0 \tag{3}$$

(2) Momentum equation:

$$\rho \frac{Du_i}{Dt} = \rho f_i - \frac{\partial P}{\partial x_i} + \mu \frac{\partial^2 u_i}{\partial x_j \cdot \partial x_j} \tag{4}$$

(3) Energy equation:

$$\rho \left(\frac{\partial T}{\partial t} + \mu_i C_p \frac{\partial t}{\partial x_i} \right) = \frac{\partial}{\partial x_i} \left(\lambda \frac{\partial T}{\partial x_i} \right) \tag{5}$$

where ρ is the density of the cooling water, u_i is the velocity, P is the pressure, T is the temperature, μ is the viscosity, C_p is the specific heat, f_i is the force per unit volume of fluid, λ is the thermal conductivity; subscripts i, j are the directions, i, j= 1, 2, 3, represents x, y, z directions, respectively; z is axial direction.

The boundary condition in Eq.(4) is that the velocity of the main inlet pipe in the simulation is 5.5 m/s. The velocity of water/wheel interface deduced with no-slip boundary condition is zero. The boundary condition is that the pressure of the main outlet pipe reduces to P_{out}=0, since pressure difference is the driving force to make water flow, and thus the calculation can be simplified.

According to Newton's law of cooling, the theoretical inter-facial heat transfer coefficient obtained by a coupling the water/roller surface is as follows.

$$h = \frac{q}{T_s - T_w} \tag{6}$$

where q is the heat flux between cooling roller and water, and T_s and T_w are the temperature of cooling roller inner wall and water, respectively.

According to Fourier's law of heat conduction,

$$q = -\lambda \frac{\partial T}{\partial x_i} \tag{7}$$

where λ is the coefficient of thermal conductivity.

1.2 Numerical simulation

In this work, the profile schematic diagram of the spinning device is illustrated in Fig. 2a. The diameter of the cooling roller (D) is 990 mm. The roller width (W) is 250 mm, and the cooling width in contract with water is 200 mm. The roller

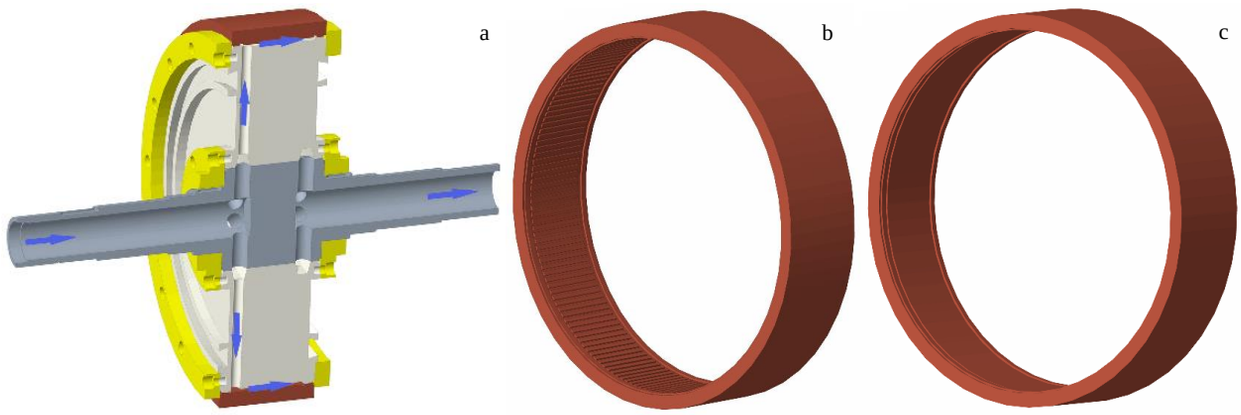

Fig.2 Profile schematic diagram of the spinning device (a) and schematics of WCS (b) and WGS (c)

thickness (*d*) is 25 mm. The rollers have the same geometric and thermal boundary conditions. The fluid flow direction is from left to right in both of the two structures. It flows from the main tube on the left to the inlet pipe in the spinning device, and then flows into the cooling area which is close to the cooling roller. The cooling area is the heat transfer section, which absorbs the heat from the cooling roller. After the cooling water absorbs the heat, it flows to the outlet pipe and into the main tube. In current engineering applications, the internal cooling structures of the roller are usually designed in two modes: water channel structure (WCS) and water gap structure (WGS) modes. The cooling area of the two structures among the inner cooling roller is different. The WCS roller is designed with more than a hundred of channels through axial direction of inner cooling roller, while the WGS roller is designed without channels. Fig. 2b and 2c illustrate the schematic of WCS and WGS roller, respectively.

The 3D mathematic model of the two cooling structures from inlet to main outlet pipe are established by the software ICEM. In this model, the outer wall is not a solid pipe, but a water/solid interface. The model is divided into several zones to improve calculation efficiency and accuracy, and each zone is discretized into all hexahedral finite element meshes. Part of the cooling structures discretized with meshes and grid refining magnifications for WCS and WGS structures are shown in Fig.3a~3d, respectively. The meshes are uniform and well-distributed, the mesh size is chosen as 0.5~2.5 mm and the total numbers of grids are 19 194 909 and 12 047 960 in the WCS and WGS structures, respectively. Most of the quality metrics criterion of the meshes is more than 0.4. The proper mesh size for obtaining a convergent solution and economizing the calculation iteration requires 700 steps.

2 Results and Discussion

Based on the above mathematic models for two kinds of internal structures, the numerical simulation was performed as described. First, the fluid flow fields and heat transfer coefficients in the cooling roller under static state are calculated, and then the calculation converges under the rotating state of the cooling roller during the process of fabricating the ribbon. The simulation at static state is converged where the residual is less than 0.001. The time for achieving heat balance of the cooling roller is about 120 s after casting, which is a short time compared to hours needed in large-scale production[16]. Since the duration of the roller rotation is a key parameter for preparing ribbons, we only present the calculated result of the rotating state of the cooling roller.

2.1 Velocity distribution in the two model structures

The fluid velocity distributions in the axial direction of the two kinds of rollers during the PFC process are shown in Fig.4. The fluid velocities in the longitudinal section of seven water channels in WCS roller are demonstrated in Fig. 4a. Since the water channels and inlet and outlet pipes are periodically arranged according to a rule of recurring for every six channels, seven channels are analyzed instead of all the channels for high efficiency. It is found that the velocity is not uniform, changing from −3.602 m/s to 2.680 m/s in the water channels. It is also found that a negative value occurs at some positions, meaning that the velocity direction is opposite: a vortex is formed at the position where the velocity is negative. Under this condition, the heat that originates from the cooling roller corresponding to the vortex cannot be taken away at the first time, thus increasing the vortex temperature. The cooling rate of this position will be lowered due to the reduced difference in temperature between cooling roller and water. Additionally, not only the velocity of each channel is not the same, but also the first channel and the seventh are not the same. Thus, the velocity is not periodic in the circumferential direction.

Fig. 4b and 4c show the velocity contour of the cooling water and its distribution on the cross-section (z=0) of the WGS structure during the PFC process, and the velocity is periodically distributed. As shown in Fig. 4b, the velocity gradually increases or decreases in the cooling area without negative value, except for the high value in the circled area at the inlet and outlet pipes. The velocity is not uniform throughout the whole water gap in the central plane z=0. It is also shown that the WGS mode can make the velocity more homogenous than the WCS mode.

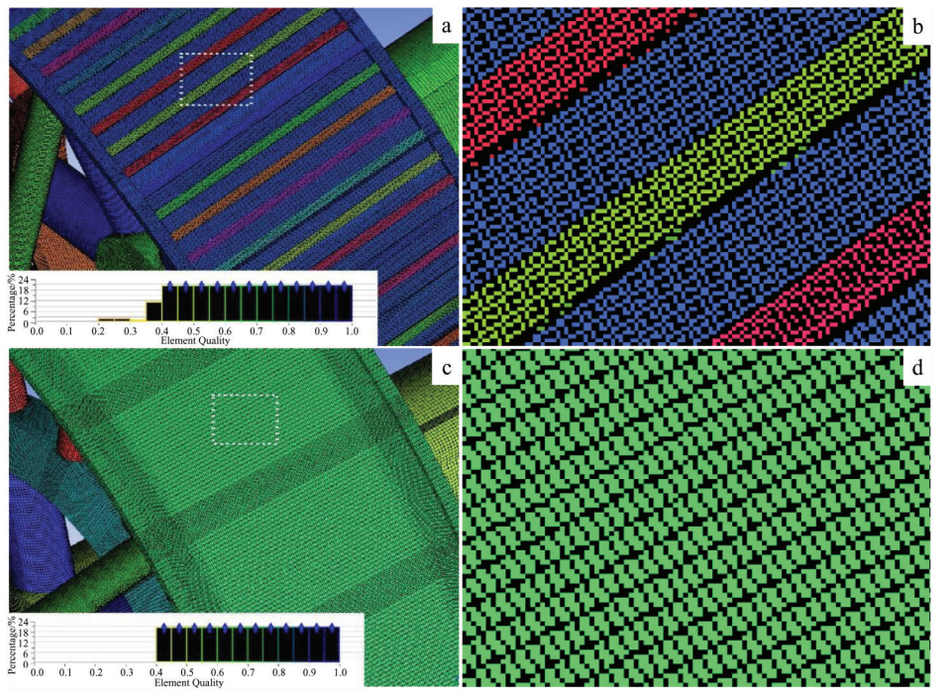

Fig.3 Part of the cooling structure discretized with meshes of WCS (a, b) and WGS (c, d) structures

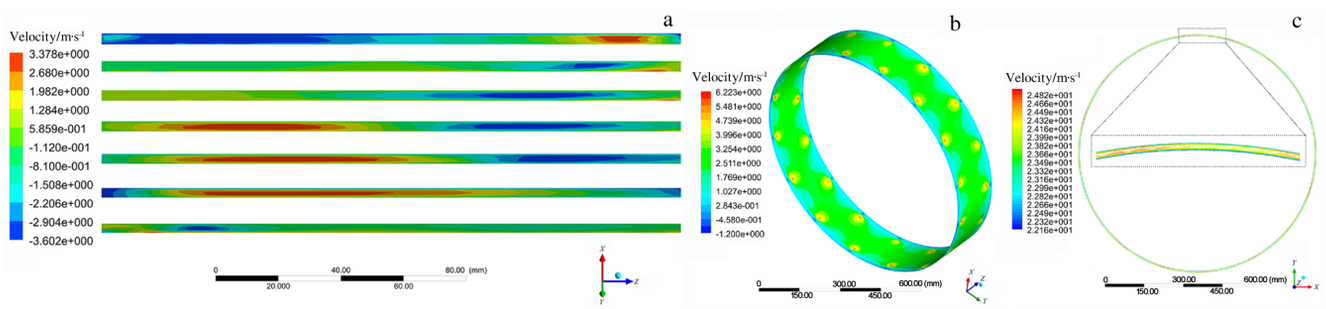

Fig.4 Velocity distribution in WCS roller (a); velocity contour (b) and velocity distribution (c) on the cross-section of z=0 of WGS roller

2.2 Streamlines in two model structures

The streamlines in the two model structures are calculated and drawn in Fig. 5. The streamline is a curve composed of different fluid particles at the same time, which gives the direction tangent to the velocity vector of different fluid particles at that time. In the WCS roller, the average velocity in the channels is 1.77 m/s, which is lower than the velocity of 2.16 m/s in the WGS roller. Thus, it is seen that water prefers to flow in the water gap instead of water channels when the roller is spinning. Fig. 5a and 5b demonstrate the streamlines of the velocities flowing into the cooling roller in the WCS and WGS rollers, respectively. It is shown that the streamlines of cooling area are not different between the two diagrams, both of which flow in the circumferential direction due to centrifugal force by roller rotation. The water is a whirlpool rotating in the main outlet pipe of the WCS roller, which has more disorder than the WGS roller. How to make the fluid flow along the axial direction needs to be resolved in the future.

2.3 Convective heat transfer coefficient distribution

The convective heat transfer coefficient h is the heat transfer capacity between two surfaces. Many researchers have assumed the heat transfer coefficient as a constant value to simplify the numerical heat transfer simulation[7,10,17-19]. However, Hui et al[20] found that the value of the heat transfer coefficient may vary in different puddle positions based on the heat conducted and coupled Naaier-Stokes equation for preparing amorphous alloys with PFC technique. It provides some references for the in-depth understanding of the convective heat transfer coefficient distribution of roller/water interface.

The Dittus-Boelter equation is used to investigate turbulent heat transfer in a tube.

$$N_{u_f} = 0.023 R_{e_f}^{0.8} P_{r_f}^{m}$$

$$m = \begin{cases} 0.4 \, (T_w > T_f) \\ 0.3 \, (T_w < T_f) \end{cases} \quad (8)$$

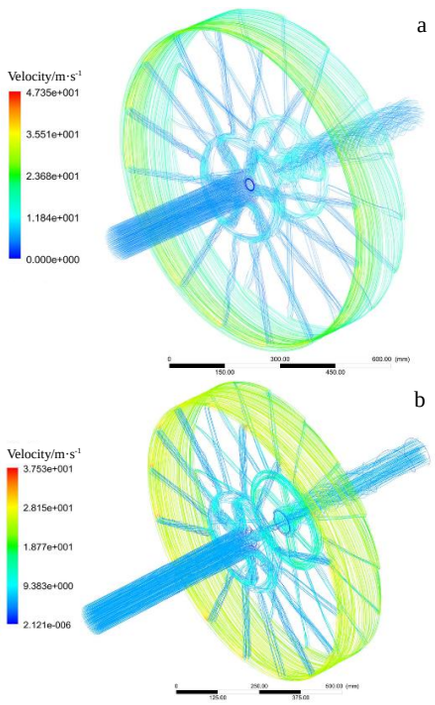

Fig.5 Streamlines in WCS (a) and WGS (b) roller

where N_{u_f}, $R_{e_f}^{0.8}$, $P_{r_f}^{m}$ are the Nusselt number, Reynolds number and Prandtl number of cooling water in water channels, respectively; T_w and T_f are the temperatures of the rotating wheel inside wall and cooling water, respectively; m is chosen as 0.4 because T_w is bigger than T_f.

$$R_{e_f} = \frac{\rho v d}{\mu} \tag{9}$$

where ρ, v, μ are the density, velocity and viscosity of the cooling water, respectively; d is the hydraulic diameter of the cooling channel.

$$P_{r_f} = \frac{C_p \mu}{\lambda} \tag{10}$$

where C_p is the specific heat, λ is the thermal conductivity.

$$N_{u_f} = \frac{hd}{\lambda} \tag{11}$$

Combining Eq.(8~11), the equation for heat transfer coefficient is expressed as

$$h = 0.023 \times \frac{\lambda}{d} \cdot \left(\frac{\rho v d}{\mu}\right)^{0.8} \cdot \left(\frac{C_p \mu}{d}\right)^{0.4} \tag{12}$$

It is shown that the cooling capacity of the WGS roller is superior to that of the WCS roller. However, it should be noticed that the above heat transfer coefficient is an average value. In our discussion, it is not appliable to identify the value of each point.

The convective heat transfer coefficient distribution curves at the roller/water interface of two model structures during the PFC process are shown in Fig.6. In Fig.6a, Line 1 to Line 7 correspond to the seven channels illustrated in Fig.4a of the WCS roller. The axial direction of the diagram shows the longitudinal direction of the channel, each line is in a prominent fluctuated status from 1×10^4 W/m^2·K to 4×10^4 W/m^2·K. Although there is a locally symmetric area in each line, the locations in the seven channels are different. We cannot find any regularity from the diagram, so it is considered that the convective heat transfer coefficient is randomly distributed.

Fig. 6b shows the convective heat transfer coefficient contours and distributions of Line 1 to Line 7 in the WGS roller at the same positions as the WCS roller for the purpose of direct comparison. We found that the convective heat transfer coefficient decreases slightly at the channel intake, then rises rapidly to a maximum value at z=−80 mm with symmetrical distribution to z=−67 mm. It drops slowly down to z=50 mm and modestly fluctuates again near the outlet. Each line has a similar trend, meaning that the distribution in the entire inner wall of the wheel is the same due to the periodic velocity distribution in the circumferential direction.

Constant h is an important factor to produce uniform thickness and wide ribbon due to the semi-empirical industrial process[21]. The maximum amount of heat from the melted metal is convected to the wheel at the coupled wall between the air and solid domain[14]. How to pin-point the position with the maximum heat flux in the internal wall of the cooling roller is a principal question. In addition, the symmetric region is in a suitable location to produce ribbon. Two locally symmetric areas are found in Fig.6b from z=−93 mm to z=−67 mm and from z=75 mm to z=90 mm. Three appropriate areas to produce ribbons are predicted with ribbon width of 26, 35 and 15 mm from left to right.

2.4 Convective heat transfer coefficient distribution

The ribbons with different widths were produced in the three areas to verify the simulation results. Seven groups of ribbons with the width of 10, 20, 30, 35, 40, 45 and 50 mm were produced. Each group was tested ten times at the three

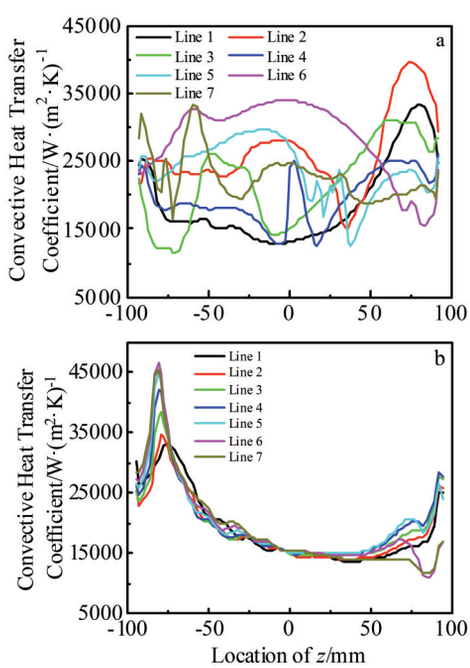

Fig.6 Convective heat transfer coefficient distribution of WCS (a) and WGS (b) roller

regions under the same conditions. If continuous production of ribbons is more than 50 kgs, we considered that the production is successful. Fig.7 shows the succeeding times of each width at the three regions. At the right area, the succeeding time decreases rapidly when the width increases to more than 20 mm. The turning points for the left and central areas are 30 and 40 mm, respectively. The scopes of ribbon widths for successful production are 30, 45 and 20 mm for the three areas from left to right, respectively. When the width reaches up to 40, 45 and 50 mm from left area to right, the succeeding time drops to zero. Both the experiment and simulation show that the central area produces the widest ribbon among the three areas. The experimentally detected width is larger than the simulation result, which may arise from some other parameters existed in the industrial production. Liu[7] and Sowjanya et al[14] found that a lower constant surface temperature of the cooling roller is an important condition to produce a continuous ribbon with uniform thickness. Therefore, regular convective heat transfer coefficient distribution should be considered as an important reference for producing wider ribbon.

2.5 Design criterion for cooling structure by thermal equilibrium principle

During the conversion of molten metal to the final ribbon product, the metal transfers heat from molten metal to water in two sequential transfer processes. The primary process consists of wheel absorbing heat and conducting inside the cooling roller. The secondary process consists of sensible heat in the wheel transferring to the water until the entire heat flow is taken away by the water.

Since the convective heat transfer coefficient is out of order in the WCS roller, thermal equilibrium can be achieved only in the primary process. Therefore, the cooling roller is the main tool to yield thermal equilibrium. Temperature difference decreases with rising mass according to equation $Q=mC_p\Delta T$. Increasing the wheel diameter may be a feasible solution to produce wider ribbons because it can reduce the temperature difference of the outer wheel surface. This is consistent with the experimental observation that the external wall temperature decreases when the roller diameter increases[16]. For this reason, some manufacturers even assembled the roller with a diameter up to 2000 mm to produce amorphous ribbons.

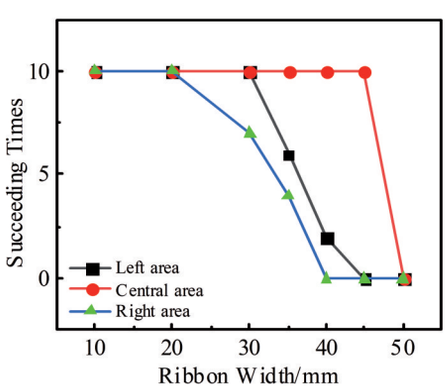

Fig.7 Succeeding times as a function of ribbon widths at three areas

Thermal convection should be the primary mode in the WGS roller based on the convective heat transfer distribution. A locally symmetric or uniform heat transfer coefficient can provide locally symmetric or uniform temperature field at the interface between the cooling roller and water. This can decrease the temperature difference of the cooling roller surface in the axial direction when the size of the cooling roller does not change. Symmetric or uniform distribution for all the convective heat transfer coefficients is the most preferred condition for the cooling structure and should be considered one of the criterions in designing the structure of a cooling roller.

3 Conclusions

1) The flow velocity of water in the cooling zone of the water channel structure (WCS) roller changes dramatically in the longitudinal direction and presents a non-periodic trend. The velocity of water in the water gap structure (WGS) roller is not uniform in the longitudinal direction, but periodic in the circumferential direction.

2) The distribution of convective heat transfer coefficients is chaotic without a certain pattern in the WCS roller. For the WGS roller, however, regular distribution and three appropriate zones with symmetric distributions are predicated. This predication has been verified by the successful production times of continuous ribbons. This finding may help to pinpoint the location where the molten is jet on the wheel.

3) The heat storage is directly proportional to the mass of the cooling roller, which provides priority to the thermal equilibrium in the WCS roller. Thermal transfer to the cooling water is considered the first factor in the WGS roller according to the thermal equilibrium principle. Uniform distribution of convective heat transfer coefficient should be a criterion in designing the structure of a cooling roller.

References

1 McHenry M E, Willard M A, Laughlin D E. *Progress in Materials Science*[J], 1999, 44(4): 291
2 Hasegawa R. *Materials Science and Engineering A*[J], 2004, 375-377: 90
3 Li F C, Liu T, Zhang J Y *et al. Materials Today Advances*[J], 2019, 4: 1
4 Enomoto Y, Tokoi H, Imagawa T *et al. Journal of the Japan Society of Applied Electromagnetics and Mechanics*[J], 2016, 24(3): 258
5 Guo S, Wang P, Zhang J C *et al. Frontiers in Energy*[J], 2019, 13: 474
6 Narasimhan M C. *US Patent*, 4142571[P], 1979
7 Liu H P, Chen W Z, Qiu S T *et al. Metallurgical and Materials Transactions B*[J], 2009, 40: 411
8 Carpenter J K, Steen P H. *Journal of Materials Science*[J], 1992, 27: 215

9 Karcher C, Steen P H. *Physics of Fluids*[J], 2001, 13(4): 834
10 Bussmann M, Mostaghimi J, Kirk D W *et al. International Journal of Heat and Mass Transfer*[J], 2002, 45(19): 3997
11 Byrne C J, Weinstein S J, Steen P H. *Chemical Engineering Science*[J], 2006, 61(24): 8004
12 Bichi A B, Smith W R, Wissink J G. *Chemical Engineering Science*[J], 2008, 63(3): 685
13 Li D R, Zhuang J H, Liu T C *et al. Journal of Materials Processing Technology*[J], 2011, 211(11): 1764
14 Sowjanya M, Kishen Kumar Reddy T. *Journal of Materials Processing Technology*[J], 2014, 214(9): 1861
15 Su Y G, Chen F L, Wu C Y *et al. Journal of Materials Processing Technology*[J], 2016, 229: 609
16 Li Y K, Yang Y, He C Y. *JOM*[J], 2018, 70(6): 855
17 Wu S L, Chen C W, Hwang W S *et al. Applied Mathematical Modelling*[J], 1992, 16(8): 394
18 Wang G X, Matthys E F. *Modelling and Simulation in Materials Science and Engineering*[J], 2002, 10: 35
19 Mattson J, Theisen E, Steen P. *Chemical Engineering Science*[J], 2018, 192: 1198
20 Hui X D, Yang Y S, Chen X M *et al. Acta Metallurgica Sinica* [J], 1999, 35(11): 1206 (in Chinese)
21 Su Y G, Chen F L, Chang C M *et al. JOM*[J], 2014, 66(7): 1277

平面流铸工艺中冷却辊流场和传热三维稳态模拟

陈　莉，李育洛，沈宁宁，惠希东
(北京科技大学 新金属材料国家重点实验室，北京 100083)

摘　要：平面流铸法是一种制备非晶和纳米晶薄带的先进技术。这项技术的难点不仅在于快速冷却以抑制薄带的晶化，还在于获得高表面质量的薄带。提出了一种用三维稳态模拟模型预测工业生产中广泛应用的2种单辊冷却结构的流场和传热系数分布的新方法。利用FLUENT软件，结合能量和动量方程，计算了2种结构的流速分布。预测了2种结构的对流换热系数分布。结果表明，水槽结构的速度分布无均匀性，也无周期性；水缝结构的速度分布无均匀性，但具有周期性。2种结构的对流换热系数分布不是中心对称的，水缝结构的冷却特性更为规则。预测了水缝结构的3个对称分布的合适区域，并通过连续生产多次验证。根据热平衡原理，描述了平面流铸法工艺的传热过程。对流换热系数的均匀分布可以作为冷却辊结构设计的依据之一。

关键词：平面流铸法；数值模拟；流场；传热；非晶和纳米晶合金

作者简介：陈　莉，女，1984年生，博士生，北京科技大学新金属材料国家重点实验室，北京 100083，E-mail：214856494@qq.com